A thin–thick transition in the surface-frozen layer of a binary alcohol mixture

E. Sloutskin and H. Kraack
Physics Department, Bar Ilan University, Ramat Gan 52900, Israel

O. Gang and B. M. Ocko
Physics Department, Brookhaven National Laboratory, Upton, New York 11973

E. B. Sirota
ExxonMobil Research and Engineering Co., Annandale, New Jersey 08801

M. Deutsch[a)]
Physics Department, Bar Ilan University, Ramat Gan 52900, Israel

(Received 18 December 2002; accepted 20 March 2003)

A new quadrilayer surface phase, and its transition to bilayer and liquid surface phases, are observed by x-ray and surface tension measurements in the surface-frozen layer of a binary mixture of $\sim 20\% C_{26}OH{:}80\% C_{18}OH$ alcohols. The surface phase diagram is rationalized qualitatively based on the free energy landscape. A quantitative elucidation of the molecular-level origin of these effects is not currently available. © *2003 American Institute of Physics.* [DOI: 10.1063/1.1574313]

The free surface of molten alcohols[1] [$H(CH_2)_nOH$, $16 \leqslant n \leqslant 28$, denoted C_nOH] was found to solidify at a temperature $T=T_s$, several degrees *above* bulk freezing at $T=T_f$. The solid surface layer, formed over the still-liquid bulk due to this surface freezing (SF) effect, was suggested to be stabilized by a delicate balance of interfacial free energies[2,3] and/or by entropic effects.[4] Normal-alkanes [$H(CH_2)_nH$, $15 \leqslant n \leqslant 50$], and their mixtures, also exhibit SF. However, while for the nonpolar alkanes a single surface-frozen monolayer is observed, for the polar alcohols a surface-frozen bilayer is obtained, stabilized by hydrogen bonds between the terminal hydroxyl groups which reside at the bilayer's center. Binary mixtures of different-length alcohols also exhibit SF within a surface phase diagram which was accounted for quantitatively by a simple thermodynamical mean-field approach.[5] In all previous studies of both pure and binary mixtures, either a single temperature-independent SF monolayer (alkanes) or a single SF bilayer (alcohols) was invariably found to form at the melt's surface, regardless of how close one gets to the bulk freezing temperature. This behavior is in marked contrast with liquid crystals, some of which exhibit a thin-layer smectic phase at the free surface of the nematic or isotropic bulk. There, the smectic layer's thickness always increases, and often diverges to macroscopic values, as the bulk transition temperature is approached.[6]

We present here an observation and study of a SF layer comprising a stack of *two* bilayers, i.e., a quadrilayer, in $C_{18}OH+C_{26}OH$ mixtures within a narrow concentration range $0.2 \lesssim \phi \lesssim 0.23$, where ϕ is the molar fraction of the $C_{26}OH$ in the liquid bulk. This phase was found in a systematic investigation, by surface tension measurements, of the dependence of the SF phase behavior on the length difference, Δn, of the two components of a binary mixtures. We focused on the transition regime between large Δn, where phase separation of the two species occurs, and the small Δn regime, where uniform mixtures are obtained. This regime was found in previous studies to show exotic phases and transitions, e.g., a surface demixing[7] or a surface rotator-to-crystal[8] transition. In the present study, the entropy changes associated with the formation of the bi- and quadrilayer surface phases were investigated by surface tension (ST) measurements. The surface-normal structure of the liquid–vapor interface was studied for the liquid, bilayer, and quadrilayer surface phases by x-ray reflectivity (XR) measurements. For a $\phi=0.2$ mixture, a temperature-driven transition from a bilayer to a quadrilayer SF phase was observed. The thermodynamics of the (ϕ,T) phase diagram, the possible mechanisms stabilizing the quadrilayer surface phase, and the free energy relations driving the various surface transitions are discussed qualitatively, though a quantitative description is still missing.

Materials, purchased from Aldrich and marked as $\gtrsim 99\%$ pure, were used as obtained. Preweighed quantities were comelted, vigorously stirred, and poured onto a preheated copper substrate. The substrate was placed inside a sealed cell, the temperature of which was regulated to $\lesssim 0.01\,^{\circ}C$. The XR measurements, at a wavelength of $\lambda = 1.54$ Å, were carried out at beamline X22B, NSLS, using the same setup as previous studies.[1,3,7,9] The technique is well-known[10] and will not be discussed here. The details of the cell, the experiment, and the data analysis were the same as in earlier studies.[1,3,5,9] The surface tension measurements were carried out using the Wilhelmy plate method, in a cell almost identical with that of the x-ray measurements. For details see Refs. 1 and 3.

The measured XR curves, $R(q_z)$ where q_z is the surface-normal wave vector transfer, are shown in Fig. 1. At $T>T_s$ (squares) a monotonically decreasing reflectivity curve, typi-

a)Author to whom all correspondence should be addressed; electronic mail: deutsch@mail.biu.ac.il

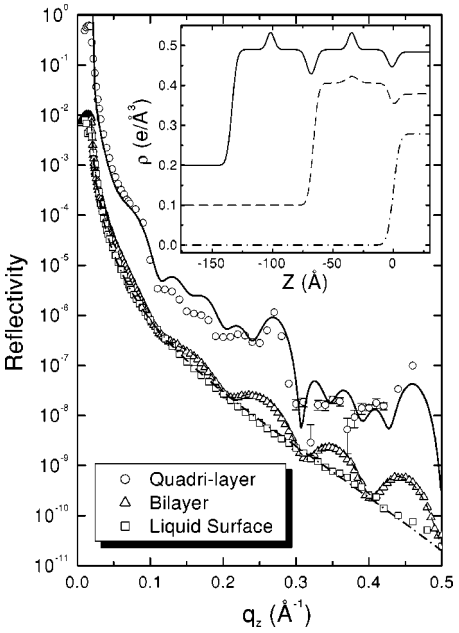

FIG. 1. The measured (points) and slab model fitted (lines) x-ray reflectivity curves for the free surface of a $C_{26}OH$ liquid surface (squares), surface frozen $C_{26}OH$ bilayer phase (triangles) and surface frozen quadrilayer phase (circles) of a 23%$C_{26}OH$:77%$C_{18}OH$ alcohol mixture melt. Inset: the electron density profiles obtained from the fit shown in the corresponding line in the main figure. Curves are shifted vertically for clarity.

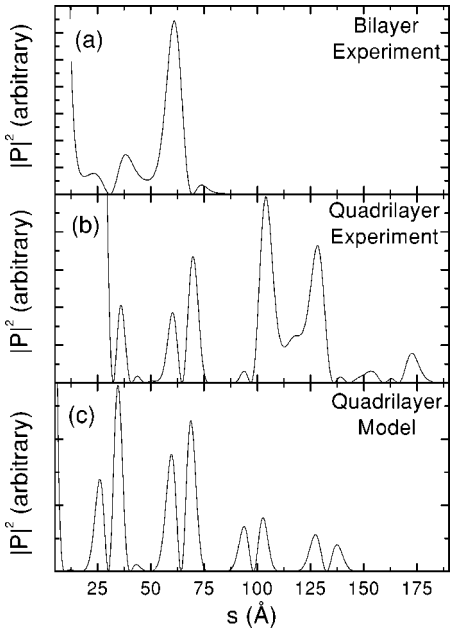

FIG. 2. The modulus squared of the Patterson function calculated from (a) the measured XR curve of $C_{26}OH$ bilayer phase, (b) the measured XR curve of the quadrilayer phase of 23%$C_{26}OH$:77%$C_{18}OH$ alcohol mixture, and (c) the slab model fitted to the quadrilayer XR curve. Note that for the usual bilayer (a) no peaks can be observed above $s=70$ Å, indicating that the largest repeat distance in the system is that corresponding to a bilayer of $C_{26}OH$. For the quadrilayer (b) and (c) the peaks extend to roughly twice larger s values.

cal of a liquid surface,[10] is obtained. Upon formation of the surface-frozen bilayer, characteristic interference fringes (triangles), akin to the Kiessig fringes in classical optics, are generated by rays reflected from the top and bottom of the bilayer. The fringe period, $\Delta q_z \approx 0.1$ Å^{-1}, indicates a layer thickness of $d=2\pi/\Delta q_z \approx 63$ Å, which agrees well with the thickness expected for a bilayer of pure ($\phi=1$) $C_{26}OH$, for which this curve was measured, taking the known[1] $\sim 22°$ molecular tilt into consideration. The XR curve shown in open circles differs strikingly from the other two. A quasi-Bragg peak is observed at $q_z \approx 0.28$ Å^{-1}, and a pronounced shoulder at ≈ 0.08 Å^{-1}. The fringes observed between these two features, albeit of low contrast, show a period which is roughly half of that observed for the bilayer (triangles in Fig. 1), indicating that this layer is about twice as thick as the single SF bilayer of pure $C_{26}OH$. The fringe period, $\Delta q_z \approx 0.045$ Å^{-1}, yields a total layer thickness of $d=2\pi/\Delta q_z = 140$ Å, roughly equal to four extended molecular lengths of $C_{26}OH$. This is consistent with the conclusion that the surface phase consists of a stack of two bilayers, i.e., a quadrilayer. The low contrast in the fringes of the quadrilayer reflectivity curve (circles) indicates a high interfacial roughness for the surface phase. Practically identical XR curves were obtained at two different temperatures, at 0.5 and 1.3 °C below T_s, within the $\Delta T = T_s - T_f \approx 1.5$ °C existence range of the quadrilayer phase. The sample was heated up to $\gtrsim 15$ °C above T_s and then recooled to the SF range below T_s in between these two XR measurements.

In view of the poor contrast in Fig. 1, it is important to consolidate the conclusion that a quadrilayer is indeed being observed without making any *a priori* assumptions about the specifics of the molecular-level structure. Thus, we have calculated the Patterson functions of the SF layers *directly from the measured XR curves* shown in Fig. 1 (circles). This is done by the method developed by Tidswell and co-workers[11] for alkylsiloxane-coated silicon. For an arbitrary surface-normal density profile the modulus of the structure factor $|\Phi(q_z)|$ is given by

$$|\Phi(q_z)|^2 = R(q_z)/R_F(q_z), \tag{1}$$

where $R_F = |(q_z - \sqrt{q_z^2 - q_c^2})/(q_z + \sqrt{q_z^2 - q_c^2})|^2$ is the Fresnel reflectivity of an ideally smooth and abrupt interface,[10] and q_c is the wave vector transfer at the critical angle for total external reflection. This $|\Phi(q_z)|^2$ was corrected below the critical angle to correspond to the wave vector value inside the bulk. Also, $|\Phi(q_z)|$ was assumed to be symmetric so that $|\Phi(q_z)|^2 = |\Phi(-q_z)|^2$. To minimize artifacts due to data termination the measured $R(q_z)/R_F(q_z)$ was extrapolated by a Gaussian from the last measured point at $q_z \approx 0.5$ Å^{-1} to $q_z = 8$ Å^{-1}, and multiplied by $\exp(-aq_z^2)$ with $a = 5$ Å^2 to minimize the influence of the outer q_z-range. The Patterson function was therefore calculated as

$$P(s) \propto \int_{-\infty}^{\infty} dq_z |\Phi(q_z)|^2 e^{-aq_z^2} e^{-iq_z s}. \tag{2}$$

This function yields peaks at values of s corresponding to repeat distances of the real-space surface-normal electron density profile. For convenience we use in the following the squared modulus of this complex function, $\mathcal{P} = PP^* = |P|^2$.

The $\mathcal{P}$ function of the $C_{26}OH$ bilayer (Fig. 1, triangles) is shown in Fig. 2(a). The internal structure of the surface frozen layer[1] results in the appearance of several peaks, rather

than a single peak corresponding only to the total thickness of the bilayer. The total thickness of the layer corresponds to the highest-s peak, $s \approx 70$ Å. The other peaks can be identified by a comparison of this $\mathcal{P}$ function with the results obtained from a slab model fit to the same bilayer in an earlier study.[1] We can see clearly that the strongest peak, located at $s=61$ Å, is due to the distance between the CH_3 slabs of the upper and the lower layers, while the OH groups' slab in the middle of the bilayer yields the two small peaks observed at low s. The published[1] total thickness of the $C_{26}OH$ SF bilayer is 65.4 Å, which is in reasonable agreement with the position of the strongest peak of the $\mathcal{P}$ function, considering the above-described extrapolations and approximations and the rather broad, $\simeq 15$ Å, width of the peaks in $\mathcal{P}$.

The $\mathcal{P}$ function obtained by the same procedure from the quadrilayer XR curve (Fig. 1, circles) is shown in Fig. 2(b). By comparison with Fig 2(a) one can readily identify the bilayer peaks in the $\mathcal{P}$ function of the quadrilayer. For a more detailed comparison note that the concentration in the surface frozen layer differs, in general, from that of the bulk, ϕ.[7] In particular, in the $C_{18}OH+C_{26}OH$ mixtures the surface frozen layer is known to consist of almost pure $C_{26}OH$ down to $\phi \simeq 0.2$.[5] Moreover, the molecules in the SF bilayer of pure $C_{26}OH$ are tilted,[1] but an admixture of $<5\%$ of $C_{18}OH$ in the liquid phase is already sufficient to cause the $C_{26}OH$ molecules in the SF phase to align along the surface normal.[5] Thus, the $d=65.4$ Å thickness of the tilted bilayer of pure $C_{26}OH$ increases to $d=65.4/\cos(22°)=70.5$ Å in the untilted bilayer of the *almost* pure $C_{26}OH$ SF layer at the surface of the $C_{18}OH+C_{26}OH$ mixture. This increase in d is observed in the upshift of the quadrilayer peak's position in Fig. 2(b) relative to that in Fig. 2(a). The most important feature in Fig. 2(b) are, however, the high-s peaks not appearing in the $\mathcal{P}$ function of the bilayer in Fig. 2(a). The outermost peaks extend up to $s \simeq 140$ Å, roughly twice the thickness of the $C_{26}OH$ bilayer, further supporting the assignment of this XR curve to a surface quadrilayer. The small peaks, extending to high-s values, decay slowly with s, and disappear totally only at $s \simeq 500$ Å. These peaks are clearly numerical artifacts, due to the small number of points and insufficient statistics of our XR data at small q_z values.

To extract structural information *at the molecular level* from the measured XR curves, we employed the widely used method[10] of approximating the surface-normal density profile, $\rho(z)$, by a physically motivated slab model, and calculating the corresponding reflectivity curve analytically through

$$R(q_z)/R_F(q_z) = |\Phi(q_z)|^2 = \left| (1/\rho_\infty) \int_{-\infty}^{\infty} \frac{d\langle \rho(z) \rangle}{dz} \exp(iq_z z)\, dz \right|^2, \tag{3}$$

where $\Phi(q_z)$ is the structure factor of the interface, ρ_∞ is electron density profile in the liquid well below the surface, and $\langle \ldots \rangle$ denotes averaging in the surface-parallel $x-y$ plane. The model $R(q_z)/R_F(q_z)$ is then fitted to the measured $R(q_z)/R_F(q_z)$. The parameters obtained from the best fit yield, in turn, the surface-normal density profiles. The model fit to the measured liquid surface $R(q_z)$ (squares), and the corresponding density profile are shown in dash-dot lines in the main Fig. 1 and the inset, respectively. As can be seen, $\rho(z)$ increases smoothly and monotonically from a zero density outside the sample, to $\rho_\infty = 0.27\ e/\text{Å}^3$ in the liquid bulk. The finite interfacial width is due to thermally excited capillary waves with a Gaussian distribution of amplitudes of width $\sigma_{\text{liquid}} \simeq 4.5$ Å, in good agreement with capillary wave theory calculations based on the surface tension of the melt.

For the bilayer we employed the same slab model used successfully for pure alcohols and alcohol mixtures.[1,5] It consists of four slabs, representing (1) the upper layer of $(CH_2)_{n-1}$ alkyl chains, (2) the OH head groups, (3) the lower layer of $(CH_2)_{n-1}$ alkyl chains [same as slab (1)], and (4) the lower-layer's terminal CH_3 groups at the SF layer-subphase interface. A semi-infinite fifth slab represents the liquid bulk subphase. Gaussian roughness was included at all interfaces. A good fit of the model (dashed line) to the measured $R(q_z)$ (triangles) is obtained as shown in Fig. 1. The corresponding density profile is shown in a dashed line in the inset, shifted up by $0.1\ e/\text{Å}^3$ for clarity. The model adopted for the quadrilayer consists of a stack of two bilayers. First attempt to fit this model to the measured $R(q_z)$ (circles in Fig. 1) yielded electron densities for the SF layer as low as that of the liquid bulk, i.e., $\sim 12\%$ lower than the densities expected and also found for all SF bilayers.[1] Moreover, the quality of the fit was poor. We therefore included in the fit an incomplete coverage of surface by the quadrilayer. A significantly improved fit was obtained for an $\sim 80\%$ coverage of the surface by the quadrilayer. The additional $\sim 20\%$ surface area was assumed to remain liquid. This model fit is shown in Fig. 1 in a solid line, with the corresponding quadrilayer $\rho(z)$, shifted up by $0.2\ e/\text{Å}^3$, shown in the inset. The average electron density of the alkyl chain slab is now much closer to that expected, but still $\sim 4\%-5\%$ lower than that of the corresponding density in pure alcohol SF bilayers. This remaining deviation can be assigned, perhaps, to the incorporation of a large number of voids and packing imperfections in the SF layer. This would reduce the liquid/solid density contrast, and, in turn, result in a reduced fringe contrast in $R(q_z)$, as indeed observed in the measured XR (circles) in Fig. 1. The incomplete coverage is also in line with the increased tendency for an imperfect packing, and the reduced contrast observed for the fringes in the $R(q_z)$ measured for the bilayer phase at $\phi \approx 0.2$.

The quality of the fit to the measured quadrilayer $R(q_z)$ is significantly inferior to that of the pure $C_{26}OH$ bilayer shown in Fig. 1. However, we believe that the model still captures the essential features of the layer's structure. A more sophisticated model could perhaps achieve a better agreement. This, however, would come at a cost of increasing significantly the number of adjustable parameters, which start showing a non-negligible degree of correlation already for our more restricted model.

It is interesting to compare the $\mathcal{P}$ function of the fitted quadrilayer slab model with that derived from the measured data. This is shown in Fig. 2(c). The peaks extend here up to $s \simeq 150$ Å, close to the high-s limit of the $\mathcal{P}$ function of the experimental data, shown in Fig. 2(b). The $\mathcal{P}$ function of the

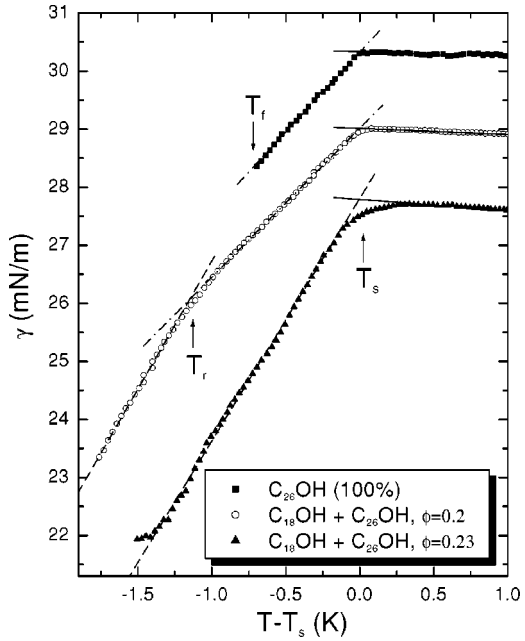

FIG. 3. Surface tension $\gamma(T)$ scans are shown for the bilayer surface phase of pure $C_{26}OH$ (squares), the quadrilayer surface phase of a 23%$C_{26}OH$: 77%$C_{18}OH$ mixture (triangles), and the 20%$C_{26}OH$:80%$C_{18}OH$ mixture (circles), where the bilayer phase is observed for $T_r<T<T_s$ and a quadrilayer for $T_f<T<T_r$. The bilayer–quadrilayer transition is clearly observed at T_r as a slope change in the 20%$C_{26}OH$:80%$C_{18}OH$ mixture curve. The lines are fits to straight lines. The curves were shifted vertically for clarity.

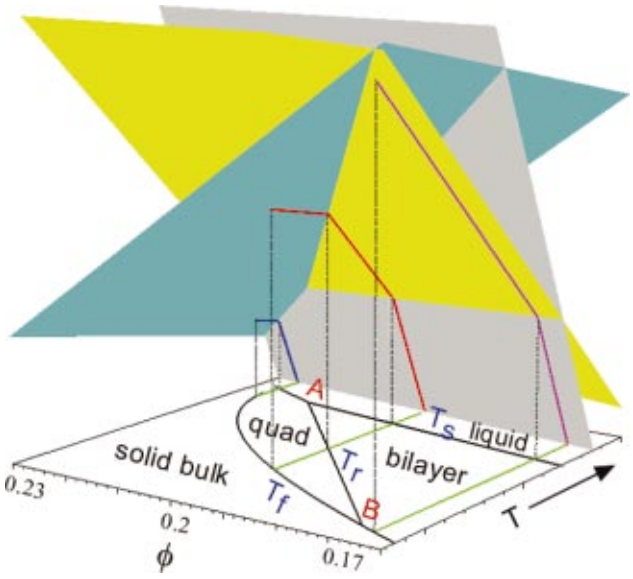

FIG. 4. (Color) Schematic representation of the free energy planes of the liquid (gray), bilayer (yellow), and quadrilayer (blue) phases. Three typical trajectories corresponding to the three $\gamma(T)$ scans shown in Fig. 2 are shown in blue, red, and violet. The projection of the plane intersections onto the (ϕ,T) plane yields the surface phase diagram. *A* and *B* denote the triple points marking the ends of the bilayer's and quadrilayer's existence range, respectively. The surface (T_s) and bulk (T_f) freezing lines and the bilayer–quadrilayer transition line (T_r) are also shown.

slab model has four split peaks. The splitting is due to the internal structure of the layers: the CH_3-depletion and the OH-enhancement slabs. The positions of the split peaks in Fig. 2(c) correspond quite well to the locations of the peaks of the experimental data's $\mathcal{P}$ function in Fig. 2(b). The differences observed are due to both the above-mentioned numerical artifacts and the simplicity of the model, which attempt to capture only the major characteristics of the structure.

Additional support for the above-presented conclusion of the formation of a SF quadrilayer at the surface comes from temperature-dependent surface tension measurements. The surface tension of a liquid, γ, is the difference between the free energies of the bulk (F_b) and of the surface (F_s). Since $F=\varepsilon-TS$, where ε is the internal energy and S the entropy of the relevant phase, $d\gamma/dT=S_b-S_s$. Thus, when a surface phase transition occurs at some $T=T_x$ between phases having different free energies, the entropy change can be obtained from the slope change in the surface tension:[3,5,9,12]

$$\Delta S_s=d\gamma/dT|_{T<T_x}-d\gamma/dT|_{T>T_x}, \tag{4}$$

assuming that the bulk entropy stays unchanged. Note, however, that, experimentally, ST is measured per unit area of the surface, so that the entropy obtained from the above-given expression is normalized to unit surface area as well. Denoting the area per molecule at the surface by A, and the entropy loss upon freezing of a single molecule by Δs_s, we obtain the number of solid layers formed at the surface as $N=\Delta S_s A/\Delta s_s$. In alcohol melts when the SF bilayer is formed at $T=T_s$, the slope of $\gamma(T)$ changes abruptly upon cooling from a low negative value for the liquid surface to a high positive value for the SF bilayer, as shown in closed squares in Fig. 3, measured for the pure $C_{26}OH$. Since the slopes below and above the transition at $T=T_s$ are 2.75 ± 0.05 and -0.09 ± 0.01 mJ m^{-2} K^{-1}, respectively, the entropy loss upon formation of a pure $C_{26}OH$ bilayer[1] is $\Delta S_s\simeq2.8$ mJ m^{-2} K^{-1}. For an earlier-determined surface molecular area of[1] $A\simeq20$ Å^2, we get here $\Delta s_s=20.3k_B$, close to the $21.7k_B$ obtained *for the bulk* by calorimetry.[3,13] The ST scans in Fig. 3 terminate at $T=T_f$, where the bulk freezing occurs and the surface tension can no longer be measured directly.

While the SF existence range, $\Delta T=T_s-T_f$, is often significantly larger in mixtures than in the pure components, the entropy almost always interpolates monotonically between those of the pure components.[5] However, for our $C_{18}OH+C_{26}OH$ mixture at $\phi\simeq0.23$ (triangles in Fig. 3) the slopes below and above T_s are 4.2 ± 0.05 and -0.19 ± 0.02 mJ m^{-2} K^{-1}, respectively, and the surface entropy change upon surface freezing is $\Delta S_s\simeq4.4$ mJ m^{-2} K^{-1}. This is much higher than the 2.8 mJ m^{-2} K^{-1} obtained here for the pure $C_{26}OH$ and the 1.82 mJ m^{-2} K^{-1} published earlier[1] for the $C_{18}OH$. Obviously, the much larger ΔS_s is due to the formation at the surface of more than a single SF bilayer, consistent with the XR-derived suggestion above that a quadrilayer, rather than a bilayer, is formed here.

Once a new solid surface phase, the quadrilayer, and a liquid–quadrilayer transition, are found, one may expect to also find, by fine-tuning ϕ and T, a solid–solid bilayer–quadrilayer surface phase transition. This expectation is based on the topology of the free energies of the different phases, shown *schematically* in Fig. 4. The gray plane, hav-

ing the highest (negative) T-slope, corresponds to the liquid phase, which has the highest entropy and therefore the lowest free energy at high temperatures. This results in the sample being liquid at high temperatures. The yellow plane, corresponding to the solid bilayer surface phase, has a lower entropy, and a smaller T-slope, than the liquid plane. The blue plane, corresponding to the solid quadrilayer surface phase, has the lowest entropy and lowest (negative) T-slope, though it is strongly tilted along the ϕ axis. The thermodynamically favored state at each specific (ϕ,T) location is always that having the lowest free energy, i.e., the lowest-lying plane at that point. The intersections between the lowest-lying planes determine the coexistence boundaries between the various phases. When projected onto the (ϕ,T) plane, these intersection lines yield the phase diagram. Our $\gamma(T)$ scans, shown in Fig. 3, correspond to trajectories parallel to the T axis at fixed ϕ values.

At low ϕ, the blue (quadrilayer) plane's high ϕ slope renders the yellow (bilayer) plane the lowest, and the quadrilayer phase does not form for $\phi \lesssim 0.18$. Only a liquid and a bilayer phase exist at the surface. Reducing T from the liquid surface phase will result in a trajectory, shown in a violet line in Fig. 4, crossing from the gray to the yellow plane at some point T_s and then reaching bulk freezing at T_f. A typical $\gamma(T)$ scan obtained along such a trajectory is shown in Fig. 3 in closed squares, and exhibits slopes characteristic of a liquid and a bilayer phase. At high ϕ the free energy topology is totally different: the high ϕ slope renders the blue plane lowest, so that upon lowering T from the liquid surface phase, a transition is observed to a quadrilayer surface phase at T_s, the intersection of the blue and gray planes. The trajectory of such a T scan at $\phi \approx 0.23$ is shown in a blue line in Fig. 4, and the corresponding $\gamma(T)$ curve is shown in closed triangles in Fig. 3. At an intermediate ϕ range between these two limits, a region must exist where the yellow plane is the lowest for part of the ΔT existence range of SF, and the blue plane is the lowest for the remaining part of ΔT. This region will terminate in two triple points, a high-T, high-ϕ one for the quadrilayer-bilayer-liquid surface phases, marked by A in Fig. 4, and a low-T, low-ϕ one for the quadrilayer-bilayer-bulk solid phases, marked by B. The line connecting these two points, marked by T_r on the (ϕ,T) plane in Fig. 4, is the boundary between the bilayer and the quadrilayer surface phases. This line must be intersected at a $T=T_r$ by any T scan in the ϕ range between the two triple points. Such a trajectory is shown in red for $\phi \approx 0.2$ in Fig. 4. The resultant $\gamma(T)$ curve, shown in open circles in Fig. 3, clearly shows the liquid–bilayer transition at T_s as well as the slope change due to the transition from a bilayer to a quadrilayer surface phase at T_r. The geometry of the phase space is such that a similar, intuitively expected, sequential bilayer-to-quadrilayer freezing transition is either preempted by T_s or by T_f in the higher- and lower-ϕ regimes. Finally, note that the ϕ range of existence of a quadrilayer vanishes at the high-ϕ end in our $C_{18}OH+C_{26}OH$ mixtures because of its preemption by bulk freezing. The preemption of the surface freezing by bulk freezing for a range of concentrations ϕ, which is often observed to occur in mixtures with large chain length mismatch Δn, is known as a ''black hole'' and has been discussed elsewhere.[5] The ϕ range of the quadrilayer phase, wedged between the ''black hole'' and the bilayer phase, is thus rather narrow, and not easily reachable in practice.

The $\gamma(T)$ scan at $\phi=0.2$, shown by open circles in Fig. 3, exhibits a liquid–bilayer surface phase transition upon cooling, with an entropy loss of $\Delta S_{s,2}=2.65 \pm 0.06\ \mathrm{mJ\,m^{-2}\,K^{-1}}$, i.e. $\Delta s_{s,2}=19.2k_B$, close to, though $\sim 5\%$ smaller than that of a SF bilayer of pure $C_{26}OH$. At $T=T_r$ a transition occurs to a region of a larger slope, so that the entropy loss relative to the liquid phase is $\Delta S_{s,4}=4.51 \pm 0.06\ \mathrm{mJ\,m^{-2}\,K^{-1}}$. Using $\Delta s_{s,2}$, this entropy loss indicates the existence of $N \simeq (4.5\times 10^{-3})\times(20\times 10^{-20})/19.2k_B \simeq 3.4$ solid layers at the surface. This result is consistent with the suggestion that the surface layer is a quadrilayer, i.e., $N \simeq 4$, particularly when considering the partial coverage, and the possibility that the entropy loss upon freezing of the inner bilayer, residing in between the liquid and the upper bilayer, is lower than that of the upper bilayer, residing between the lower bilayer and the vapor phase.

The liquid–bilayer surface transitions in both $\gamma(T)$ scans shown in Fig. 3 (closed squares and open circles) are abrupt. The sharp discontinuity at $T=T_s$ in $d\gamma/dT$, and hence in $\Delta S(T)$, was also found in previous studies of the SF transition,[3,5,14] and is indicative of a first-order phase transition. The bilayer–quadrilayer transition at $T=T_r$ (open circles) and the liquid–quadrilayer transition at $T=T_s$ (closed triangles) in Fig. 3 appear to be rounded. Since no second-order transitions were found to date in SF layers, these transitions are probably still first order, and the rounding could be caused by impurity or kinetic smearing. Similar smearing was observed in bulk crystallization in binary mixtures, where small amounts of uncrystallizable materials were found to cause a rounded transition, and also a reduced crystallinity at low temperatures.[15] The last effect, in particular, is the three-dimensional analogue of the partial surface coverage by the SF phase observed here. A more definite determination of the order of the transition will require purer samples and careful bidirectional measurements of the transitions discussed here.

Two questions arise concerning somewhat related issues: why does the quadrilayer form at the surface at this particular mixture, and what stabilizes the quadrilayer at the surface against inducing a complete solidification of the bulk. To answer the first question, we note that for mixtures where the length difference of the two molecules, Δn, is small, the effective layer thickness, and thus the XR fringe period, vary continuously with ϕ between the values of the pure components.[5] For large Δn, however, phase separation usually occurs at the surface and the SF layer is composed almost exclusively of the longer component. In the transition region between the two regimes, at $\Delta n/\bar{n} \approx 0.4$, where $\bar{n}$ is the average of the lengths of the two molecules, exotic phases were found, as mentioned earlier. In the present case $\Delta n/\bar{n} \approx 0.36$ just at the transition between the two regimes. Thus, we also find here for $\phi \approx 0.23$ an exotic surface phase, the quadrilayer, whose existence is demonstrated by an anomalously high entropy loss upon surface freezing, and a markedly different XR curve, shown in circles in Fig. 1, both

of which are shown above to be consistent with the formation of a double bilayer at $T=T_s$.

What stabilizes the solid quadrilayer at the free surface of the melt? In studies of SF in monocomponent alkanes and alcohols, it was proposed that the formation of a solid monolayer (or bilayer) *at the surface* lowers the overall surface free energy relative to that of a liquid surface, thus stabilizing the SF phase at a temperature where the bulk is still liquid.[1,2] However, the same argument cannot be used for the formation of an additional bilayer, since if the formation of a second bilayer, which is not at the surface, lowers the total free energy further, so should additional bilayers, and bulk solidification should ensue. It is possible, in principle, that the surface field will have a decay length larger than the thickness of a single mono- or bilayer. In this case the surface field strength at consecutive layers will vary with depth below the surface, approaching eventually zero in the bulk. For a decay length larger than a single bilayer but smaller than, say, three bilayers, it is possible that the surface field will stabilize two SF bilayers, i.e., a quadrilayer, at the surface, but not three or more, and hence bulk crystallization will not occur. A related phenomena occurs in liquid crystals where even more layers can form.[6] In that case, however, the increase in the number of surface layers upon cooling is strictly sequential, while here it is also possible to vary ϕ to reach regions in phase space where the transition is directly from a liquid either to a bilayer or to a qaudrilayer. The difference in the range of the surface field between monocomponent alkane melts, where the surface field does not extend beyond a single layer, and the present case, where it extends to two bilayers, may stem from the fact that in the present mixture we are close to the edge of a ''black hole'' where the surface free energy balance just barely favors SF over bulk freezing. The above-noted arguments are admittedly speculative. Additional experimental evidence as well as a quantitative theoretical formulation are required to elucidate the origin of the quadrilayer formation. Such results may lead also to the detection of phases with more SF layers than those detected so far.

In conclusion, a first observation (by XR and ST measurements) of a surface-frozen quadrilayer phase is reported. It was found to occur in melts of $C_{18}OH+C_{26}OH$ mixtures for concentrations near $\phi=0.23$. The observed surface phases and transitions were shown to emerge from the topology of the (F,ϕ,T) space. The liquid–bilayer transition is sharp and thus seems to be first order, as found for SF in many other pure alcohols and alcohol mixtures. The liquid–quadrilayer and the bilayer–quadrilayer transitions are somewhat rounded, most probably due to impurity or kinetic smearing, although the possibility of a second-order transition cannot be ruled out at present. The thermodynamics stabilizing the solid quadrilayer at the surface requires further study.

We thank the NSLS for beamtime allocation at X22B. BNL is supported by the U.S. DOE under Contract No. DE-AC02-98CH10886.

[1] O. Gang, X. Z. Wu, B. M. Ocko, E. B. Sirota, and M. Deutsch, Phys. Rev. E **58**, 6086 (1998); O. Gang, B. M. Ocko, X. Z. Wu, E. B. Sirota, and M. Deutsch, Phys. Rev. Lett. **80**, 1264 (1998).
[2] E. B. Sirota, X. Z. Wu, B. M. Ocko, and M. Deutsch, Phys. Rev. Lett. **79**, 531 (1997).
[3] B. M. Ocko, X. Z. Wu, E. B. Sirota, S. K. Sinha, O. Gang, and M. Deutsch, Phys. Rev. E **55**, 3164 (1997); X. Z. Wu, B. M. Ocko, E. B. Sirota, S. K. Sinha, M. Deutsch, G. H. Cao, and M. W. Kim, Science **261**, 1018 (1993).
[4] A. V. Tkachenko and Y. Rabin, Phys. Rev. Lett. **76**, 2527 (1996); Phys. Rev. E **55**, 778 (1997); Phys. Rev. Lett. **79**, 532 (1997).
[5] E. Sloutskin, E. B. Sirota, H. Kraack, O. Gang, A. Döerr, B. M. Ocko, and M. Deutsch, J. Chem. Phys. **116**, 8056 (2002); E. Sloutskin, O. Gang, H. Kraack, A. Doerr, E. B. Sirota, B. M. Ocko, and M. Deutsch (unpublished).
[6] P. S. Pershan, *Structure of Liquid Crystal Phases* (World Scientific, Singapore, 1988); P. S. Pershan and J. Als-Nielsen, Phys. Rev. Lett. **52**, 759 (1984); B. M. Ocko, A. Braslau, P. S. Pershan *et al.*, *ibid.* **57**, 94 (1986).
[7] E. Sloutskin, O. Gang, H. Kraack, B. M. Ocko, E. B. Sirota, and M. Deutsch, Phys. Rev. Lett. **89**, 065501 (2002).
[8] X. Z. Wu, B. M. Ocko, H. Tang, E. B. Sirota, S. K. Sinha, and M. Deutsch, Phys. Rev. Lett. **75**, 1332 (1995).
[9] E. Sloutskin, E. B. Sirota, H. Kraack, B. M. Ocko, and M. Deutsch, Phys. Rev. E **64**, 031708 (2001).
[10] J. Als-Nielsen and D. McMorrow, *Elements of Modern X-Ray Physics* (Wiley, New York, 2001); M. Deutsch and B. M. Ocko, in *Encyclopedia of Applied Physics*, edited by G. L. Trigg (VCH, New York, 1998), Vol. 23, p. 479.
[11] I. M. Tidswell, B. M. Ocko, P. S. Pershan, S. R. Wasserman, G. M. Whitesides, and J. D. Axe, Phys. Rev. B **41**, 1111 (1990).
[12] G. L. Gaines, *Insoluble Monolayers at the Liquid Gas Interface* (Wiley, New York, 1966); G. Roberts, *Langmuir-Blodgett Films* (Plenum, New York, 1990), p. 108.
[13] E. B. Sirota and X. Z. Wu, J. Chem. Phys. **105**, 7763 (1996).
[14] N. Maeda and V. V. Yaminsky, Phys. Rev. Lett. **84**, 698 (2000).
[15] E. B. Sirota, J. Chem. Phys. **112**, 492 (2000).